Brain-targeting, acid-responsive antioxidant nanoparticles for stroke treatment and drug delivery

Shenqi Zhang [a,e,1], Bin Peng [a,1], Zeming Chen [a], Jiang Yu [a], Gang Deng [a], Youmei Bao [a], Chao Ma [a], Fengyi Du [a], Wendy C. Sheu [b], W. Taylor Kimberly [f], J. Marc Simard [g], Daniel Coman [c], Qianxue Chen [e], Fahmeed Hyder [b,c], Jiangbing Zhou [a,b,*], Kevin N. Sheth [a,d,**]

[a] *Department of Neurosurgery, USA*
[b] *Department of Biomedical Engineering, USA*
[c] *Department of Radiology and Biomedical Imaging, USA*
[d] *Department of Neurology, Yale University, New Haven, CT, 06510, USA*
[e] *Department of Neurosurgery, Renmin Hospital of Wuhan University, Wuhan, Hubei, 430060, China*
[f] *Department of Neurology, Division of Neurocritical Care, Massachusetts General Hospital, Boston, MA, USA*
[g] *Department of Neurosurgery, University of Maryland School of Medicine, Baltimore, MD, 21201, USA*

ARTICLE INFO

ABSTRACT

Stroke is the leading cause of death and disability. Currently, there is no effective pharmacological treatment for this disease, which can be partially attributed to the inability to efficiently deliver therapeutics to the brain. Here we report the development of natural compound-derived nanoparticles (NPs), which function both as a potent therapeutic agent for stroke treatment and as an efficient carrier for drug delivery to the ischemic brain. First, we screened a collection of natural nanomaterials and identified betulinic acid (BA) as one of the most potent antioxidants for stroke treatment. Next, we engineered BA NPs for preferential drug release in acidic ischemic tissue through chemically converting BA to betulinic amine (BAM) and for targeted drug delivery through surface conjugation of AMD3100, a CXCR4 antagonist. The resulting AMD3100-conjugated BAM NPs, or A-BAM NPs, were then assessed as a therapeutic agent for stroke treatment and as a carrier for delivery of NA1, a neuro-protective peptide. We show that intravenous administration of A-BAM NPs effectively improved recovery from stroke and its efficacy was further enhanced when NA1 was encapsulated. Due to their multifunctionality and significant efficacy, we anticipate that A-BAM NPs have the potential to be translated both as a therapeutic agent and as a drug carrier to improve the treatment of stroke.

1. Introduction

Stroke is a leading cause of mortality and morbidity worldwide [1]. Intravenous administration of thrombolytic tissue-type plasminogen activator (tPA) within 4.5 h of symptom onset remains the only effective FDA-approved treatment [2]. With this narrow therapeutic window, only 7% of patients are eligible for the treatment [3]. tPA carries risk of hemorrhagic transformation, and treated patients still suffer considerable disability. The lack of additional pharmacotherapies for stroke can be attributed to two major reasons. First, most therapeutics cannot

efficiently penetrate the brain due to the existence of the blood brain barrier (BBB) [4]. Although the BBB is partially disrupted after ischemic insult, the degree of disruption is not enough to allow for delivery of pharmacologically significant quantities of drugs to the brain for effective treatment [5,6]. Second, single agent pharmacotherapy is insufficient and effective treatment of stroke likely requires multiple complementary targets [7]. Development of new pharmacotherapies with improved brain penetration and therapeutic benefits for stroke treatment persists as a major public health need.

We recently reported a group of natural small molecule-based nanomaterials isolated from medicinal plants that can self-assemble into NPs [8–11]. Among them, betulinic acid (BA) forms rod-shaped NPs and can effectively improve post-stroke recovery as an antioxidant agent. Additionally, the NPs can be employed as a carrier to enhance drug delivery to the ischemic brain [10]. However, BA NPs as a carrier have two limitations. First, BA NPs release payload at a slow rate at physiological pH. Less than 30% of encapsulated drugs are released in the first 24 h, with complete drug release requiring over 6 days [10]. Controlled drug release at a slow rate is beneficial for some diseases but may not be optimal for acute stroke due to its narrow therapeutic window. There is an additional concern if drugs that are designed for the acute phase induce unwanted side effects when presented over a long time. Second, BA NPs penetrate the brain largely through the disrupted BBB and thus have limited penetrability and specificity for the broader ischemic region including the infarct core and penumbral tissue.

In this study, we sought to develop a new generation of antioxidant NPs that are capable of releasing payload at an accelerated rate while also demonstrating efficient penetration in the ischemic brain. To this end, we screened a collection of natural antioxidant nanomaterials, including BA, lupeol (LP), glycyrrhetic acid (GA), sumaresinolic acid (SA), stigmasterol (ST), dehydrotrametenolic acid (DTA), oleanolic acid (OA), ursolic acid (UA), poricoic acid (PAA), and β-sitosterol (BT). Among them, BA [10], LP [12], GA [13], ST [14], OA [15], and UA [16] were reported to be active for stroke treatment when administrated as free drug. Through the screen, we identified BA as one of the most potent candidates for stroke treatment. Using magnetic resonance spectroscopic imaging (MRSI), we showed that the ischemic brain is acidic with pH ranging from 6.0 to 6.8. To enable accelerated drug release preferentially in the ischemic brain, we chemically converted BA to betulinic amine (BAM) and found that NPs consisting of BAM had accelerated drug release in acidic conditions. To enhance brain penetration, we selected a BAM NP formulation for further engineering through surface conjugation of AMD3100, which interacts with CXCR4 that are preferentially enriched in the ischemic tissue [17]. We characterized the resulting AMD3100-conjugated BAM NPs, or A-BAM NPs, as a therapeutic agent for stroke treatment and as a carrier for delivery of NA1. NA1, or Tat-NR2B9c, is a fusion peptide designed to protect neurons against NMDA receptor-mediated excitotoxicity [18]. NA1 was recently evaluated and demonstrated therapeutic benefits in stroke patients but not in those who also received tPA infusion [19]. While tPA interaction resulted in an overall neutral trial, translational efforts have continued in ongoing phase III trials. We found that intravenous administration of A-BAM NPs effectively improved the recovery of mice from stroke, and their efficacy was further significantly improved when NA1 was encapsulated. We showed that the therapeutic benefit of NA1 was not reduced by co-infusion of tPA when delivered via A-BAM NPs. These findings suggest A-BAM NPs as both an effective agent for stroke treatment and an efficient carrier for targeted delivery of therapeutics to the ischemic brain.

2. Materials and methods

2.1. Materials

BA was purchased from Cayman Chemical, AMD3100 tetrahydrochloride was purchased from Santa Cruz Biotechnology. MAL-PEG2000-NHS were obtained from JenKem Technology. All other chemicals were purchased from Sigma-Aldrich.

2.2. Synthesis of BAM and NPs

For synthesis of BAM, triethylamine (1.76 mmol, 2.0 eq) and compound **1** (Fig. 2a) (1 mmol, 1.2 eq) were added to a mixture of BA (0.88 mmol, 1.0 eq), EDCI (1.1 mmol, 1.3 eq), HOBt (1.1 mmol1.3 eq) in dichloromethane (5 ml). The mixture was stirred overnight at room temperature under N_2. The solvent was evaporated under reduced pressure and the residue was purified by silica gel column chromatography (Hexane-EtOAc gradient elution, 5%–30%) for intermediate **3** (Fig. 2a). To a mixture of compound **3** (Fig. 2a) in EtOAc (3 ml) and MeOH (1 ml) was added concentrated hydrochloric acid (0.6 ml) at 0 °C for 30 min. It was then stirred overnight at room temperature. The resulting suspension was concentrated, filtered, and washed with EtOAc and dichloromethane to obtain the white solid (320 mg, total yield 67%).

BAM NPs were synthesized using the standard emulsion procedures [20,21]. For typical synthesis of BAM NPs encapsulated with hydrophobic cargos, including IR780, coumarin 6 (C6), and NA1, the selected cargo was dissolved together with 5 mg BAM in mixed organic solution of DCM (0.95 ml) and Methanol (0.05 ml) and added dropwise to a solution of 4 ml 2.5% PVA (aqueous phase). The resulting emulsion was sonicated on ice for 40 s (5 s on, 5 s off) and added to a stirring solution of 0.3% PVA in water (aqueous phase, 50 ml). After evaporation at 4 °C overnight, BAM NPs were collected by centrifugation at 18,000 rpm for 30 min. Then, the pellets were suspended in 40 ml of water to remove residual PVA and collected by centrifugation at 18,000 rpm for 30 min to obtain the NPs. Finally, NPs were suspended with 5 ml of water, sonicated for 3 min, and then lyophilized for storage. BAM NPs were obtained with surface display of maleimide groups through chemical modification with MAL-PEG2000-NHS. AMD3100 was conjugated according to our previously reported method [17].

2.3. Nuclear magnetic resonance (NMR)

NMR spectra were recorded on A400c Agilent DD2 400 MHz NMR Spectrometer with AS7620 96-sample changer (Autosampler). Chemical shifts were reported in parts per million (ppm) and referenced to the residual deuterated solvent.

2.4. Liquid chromatography mass spectrometry (LCMS)

LCMS spectra were recorded on Shimadzu 9030 Quadrupole Time-of-Flight High-Performance Liquid Chromatograph Mass Spectrometer. Samples in methanol were injected into Shim-pack Scepter C18 column (1.9 μM, 2.1 × 100 mm) using acetonitrile with 0.1% Formic Acid (FA) and Water (0.1% FA) as solvents. Mass spectra are recorded in positive ion mode.

2.5. Scanning electron microscopy (SEM)

The morphology of NPs was determined by SEM. Briefly, lyophilized NPs were mounted on a carbon tape and coated with gold using a sputter with current at 40 mA (Dynavac Mini Coater, Dynavac, USA). The images were carried out by a LaB electron gun with an accelerating voltage of 3 kV using a Philips XL 30 SEM.

2.6. Transmission electron microscope (TEM)

The structure of NPs was determined by TEM. NPs resuspended in 10 μL water were applied to holey carbon-coated copper grids (SPI, West Chester, PA, USA). A filter paper was used to absorb the NPs after 5 min. The grids were left at fume hood until completely dried and then visualized by using a JEOL 1230 transmission electron microscope (JEOL

Ltd., Japan) at 100 kV.

2.7. Dynamic light scattering (DLS)

The hydrodynamic size and zeta potential of NPs were measured by DLS. Briefly, 0.1 mg NPs in 1 ml ddH2O water was added to a transparent cuvette, which was subjected to measurement using a Malvern Zetasizer.

2.8. Characterization of drug loading and release

For characterization of drug loading, selected NPs were dissolved in DMSO to release agents, which were quantified by a BioTek microplate reader for IR780 or NA1. For characterization of drug release, NA1-A-BAM NPs were placed into a dialysis bag (MWCO 3000) against PBS in pH 6.5 or pH 7.4 and immersed into 30 mL PBS in a prepared tube under a predetermined sink condition. The tubes were kept at room temperature with a shaking speed at 100 cycles/min. At selected time intervals from 0.5 to 48 h, 1 mL of solution outside the dialysis bag was taken out and replaced with the same volume of fresh medium. NA1 in the sampled solution was quantified by a BioTek microplate reader. The cumulative NA1 release was calculated and plotted against time.

2.9. Characterization of acid-responsiveness

To characterize the response to acid, 1 mg/mL NPs were incubated in pH 6.5 or pH 7.4 at 37 °C. SEM was used to detect the time-dependent size distribution and morphological change with time.

2.10. Middle cerebral artery occlusion (MCAO) model and imaging

Male Wistar rats (Charles River Laboratories), ~200 g each, and male C57BL/6 mice (Charles River Laboratories), ~20 g each, were given free access to food and water before all experiments. All animal experiments were approved by the Yale University Institutional Animal Care and Utilization Committee. Other than the study for MRSI, in which rats were utilized, mice were used in all others. MCAO models were generated according to methods that we recently reported [22,23]. Successful MCA occlusion was confirmed by a reduction of rCBF by over 80% measured by laser Doppler flowmetry. The occlusion lasted 90 min and the monofilament was withdrawn to allow for reperfusion. Imaging of IR780-loaded NPs was also carried out using IVIS (Xenogen) according to the same procedures described in our previous publication [20,22]. To correlate the location of NPs and ischemic region, the brains were sliced coronally with 2 mm thickness and stained with TTC by incubating the brain sections in a 2% TTC solution for 20 min at 37 °C. The images of the TTC staining and the IR780 fluorescence were captured with a camera and IVIS imaging system, respectively. For imaging NPs and co-colocalization with CXCR4, MCAO mice were intravenously administered with C6-loaded A-BAM NPs. Twenty fours later, the mice were perfused with 1 × PBS followed by 4% paraformaldehyde (PFA). The brains were incubated overnight in 4% PFA. Thick sections of 30 μm were obtained using a vibratome (Leica). After blocking with 4% BSA for 30 min and washing for 3 times, the sections were incubated with CXCR4 (1:200, Novus NB100-74396) for overnight at 4 °C. The sections were incubated with Donkey anti-Rabbit IgG (ab150075, Abcam) for 30 min and washed by PBS for 3 times. The samples were mounted and imaged using a confocal microscope (Leica TCS SP8).

2.11. pH imaging in vivo

All magnetic resonance data were acquired using an 11.7 T Bruker horizontal-bore spectrometer. MCAO mice underwent T_2-weighted MRI to localize the ischemic lesion using a spin-echo sequence with TR 6000 ms and 10 TE (10–100 ms), FOV 25 × 25mm^2, matrix 128 × 128, and slice thickness 1 mm. During imaging, the body temperature was

maintained using a circulating warm water heating pad and paralube vet ointment was applied to the eyes to prevent dryness. For the pH imaging with BIRDS, which require the administration of a contrast agent TmDOTP^{5-}, a tail vein infusion line was inserted prior to the experiment. During this procedure, the animal was anesthetized with 3% isoflurane and placed on a heating pad to maintain body temperature. A 30G needle was inserted into PE10 (Braintree Scientific, LLC) line and filled with heparinized saline. The needle was inserted into the lateral tail vein and checked for backflow to ensure correct placement within the vein, prior to being anchored to the tail with tape. Heparinized saline (~50 μL) was flushed through the line approximately every 20 min throughout the remainder of the imaging session to ensure proper functioning of the infusion line and to prevent clotting. The animal was placed in a prone position with the head underneath a 1.4 cm surface RF coil. The animal and coil were then placed in the isocenter of the magnet bore. Body temperature was monitored using a rectal fiber-optic temperature probe and breathing rate was monitored using a respiratory monitor. For pH$_e$ measurements with BIRDS, 100 mg/kg probenecid was administered over 10 min and followed after 20 min by a co-infusion of 100 mg/kg probenecid and 1 mmol/kg TmDOTP^{5-}. Probenecid was used to increase the plasma concentration of the circulating contrast agent and reduce its rate of renal clearance. All infusions were performed using a syringe pump at a rate of 15 μL/min for a total infusion time of 100 min. Chemical shift imaging for BIRDS began 45 min after the start of the infusion. The H2, H3 and H6 chemical shifts of TmDOTP^{5-} are pH$_e$-dependent and were used to calculate the pH$_e$ within each voxel at an isotropic resolution of 1 mm^3 as previously described [24–26] (R).

2.12. Determination of the therapeutic benefits

Mice received MCAO surgery and were randomly divided into four groups (n = 7), which received treatment of phosphate-buffered saline (PBS), blank A-BAM NPs, NA1-A-BAM NPs at a dose equivalent to 1 nM/g of NA1, and the same amount of free NA1, respectively. Mice received three injections, which were given intravenously at 0, 24, and 48 h after surgery. For experiments involved with tPA, tPA (Activase (alteplase), Genentech) was dissolved in sterile water and administered as an intravenous bolus injection of 1 mg/kg followed by a 9 mg/kg infusion for 30 min, started at 1.5 h after MCAO, with a syringe infusion pump (World Precision Instruments). Afterward, the mice were monitored for survival for 14 days and euthanized if one of the following criteria was met: 1) the mouse's body weight dropped below 15% of its initial weight, or 2) the mouse became lethargic or sick and unable to feed. For the study to determine the impact of treatments on infarct volume and neurological score, another cohort of mice was prepared (n = 5) and received the same treatments as described above. 3 days later, the neurological score of each mouse was assessed by a standard behavioral test [5,10], and was scored as follows: 1) normal motor function, 2) flexion of torso and contralateral forelimb when animal was lifted by the tail, 3) hemiparalysis resulting in circling to the contralateral side when held by tail on flat surface, but normal posture at rest, 4) leaning to the contralateral side at rest, and 5) no spontaneous motor activity. Therapeutic evaluations were carried out using an unbiased approach; the reviewer who scored mouse function was unaware of which treatment group each mouse belonged to. After the evaluation, the mice were sacrificed and the brains were excised, sectioned, and stained with TTC. The infarct area in each slice was quantified using Image J (NIH).

2.13. Statistical analysis

All data were collected in triplicate and reported as mean and standard deviation. Comparison between the groups was performed using a *t*-test. One-way ANOVA was used to analyze multiple comparisons by GraphPad Prism 7.0. $P < 0.05$ (*), 0.01 (**), 0.001 (***) and 0.0001 (****) were considered significant.

3. Results

3.1. Experimental design

We started with a screen of a collection of antioxidant nanomaterials and identified BA as one of the top candidates for stroke treatment. Afterward, we engineered BA NPs for drug delivery to the ischemic brain. Specifically, to enable accelerated drug release and enhanced penetration specifically to the ischemic brain, we chemically converted BA to BAM and selected a BAM formulation for further engineering through surface conjugation of AMD3100 (Scheme 1). Last, we evaluated the resulting A-BAM NPs as both therapeutic agent and carrier for NA1 delivery for stroke treatment in mice receiving MCAO surgery (Scheme 2).

3.2. Screen of natural nanomaterials for stroke treatment

We recently developed a magnetic NP- based chemical extraction approach, through which we isolated and identified a group of natural small molecule-based nanomaterials, most of which are known to have antioxidant activities [8–11]. To identify one suitable for stroke treatment, we selected and evaluated 10 of those identified nanomaterials, including BA, LP, GA, SA, ST, DTA, OA, UA, PAA, and BT. BA, which we previously demonstrated to be effective for stroke treatment [10], was used as a benchmark for comparison. Similar to BA, ST, DTA, PAA and BT formed rod-shaped NPs with a diameter of 60–100 nm and a length of ~400 nm; the rest formed spherical NPs with diameters ranging from 120 to 220 nm (Fig. 1a and b). All NPs exhibited negative surface charge with zeta potential ranging from −18 to −25 mV. To determine their therapeutic effects, NPs were intravenously administered to mice with MCAO. NPs were given at 2 mg/injection for three times at 0, 24, and 48 h after surgery. Three days later, the mice were euthanized. Their brains were isolated and subjected to triphenyltetrazolium chloride (TTC) staining. We found that all the tested NPs demonstrated various degrees of effect on reducing infarct size, and, among them, BA NPs and SA NPs are the most efficacious (Fig. 1c, Fig. S1, Supporting Information). As BA NPs have demonstrated great promise in our previous study [10], we chose BA for further optimization through chemical modification to enable formation of NPs for accelerated drug release in ischemic brain tissue.

### 3.3. Synthesis and characterization of acidic pH-responsive BA NPs

Ischemic insults alter the metabolism in the ischemic brain by switching it from aerobic to anaerobic glycolysis, leading to the accumulation of lactate and protons, which together reduce pH [27–31]. To measure the pH distribution in the ischemic brain, we employed biosensor imaging of redundant deviation in shifts (BIRDS), a molecular imaging platform which we recently developed to detect extracellular pH based on the chemical shift information via MRSI [25], and has been successfully used to measure pH reductions in brain and liver cancers in

vivo [24,32,33]. We found that the ischemic region in the brain is acidic, with pH ranging from 6.0 to 6.8, and the acidosis lasted for over 2 days; in contrast, the pH in the contralateral normal tissue remains neutral (Fig. 2b).

NPs consisting of BA are stable in acidic and physiological conditions, while disassembled in a fast rate at alkaline pH (Fig. 2d, Fig. S2, Supporting Information). To enable accelerated degradation in acidic conditions, we chemically modified BA to BAM by converting the carboxyl group on the edge of BA ring to an amino-terminal group (Fig. 2a). Successful synthesis of BAM was confirmed by ^{1}H NMR (400 MHz, DMSO-d_6), ^{1}H–^{1}H COSY and liquid chromatography mass spectrometry (LCMS) (Fig. S3, Supporting Information). We found that BAM formed NPs in various size and shape, and the morphology of NPs improved with incorporation of BA (Fig. S5a, Supporting Information). Unlike BA NPs, which were responsive to alkaline pH, NPs consisting of BAM responded to acidic pH by releasing payloads in an accelerated rate (Fig. 2c, Figs. S5b and c, Supporting Information). Although further investigation is needed, the acid responsiveness is likely driven by protonation of amino groups, which increases the repulsive force within BAM NPs and destabilizes the NP structure. Due to the uniform morphology and acid-triggered drug release property, NPs consisting of 75% BAM and 25% BA were chosen for further study. To simplify the nomenclature, we designated the NPs as BAM NPs. Analysis by SEM showed that BAM NPs were unstable in acidic buffer and partially disintegrated within 24 h, while BA NPs maintained their structure in the same conditions (Fig. 2d).

3.4. Engineering BAM NPs for targeted delivery to the ischemic brain

In seeking molecular targets for selective delivery of BAM NPs to the ischemic brain, we focused on CXCR4, a chemokine receptor highly expressed in the brain after ischemic insult [17]. The preferential expression of CXCR4 in the ischemic region but not others was confirmed by Western Blot and immunostaining (Fig. 3a and b). To enable CXCR4 targeting, we conjugated AMD3100 to the surface of BAM NPs via a heterobifunctional polyethylene glycol (PEG) linker, NHS-PEG-Mal. AMD3100 is an antagonist of CXCR4, which have been recently explored for CXCR4-targeted drug delivery [17,34,35]. Successful conjugation was confirmed by amine depletion analysis through the classical ninhydrin reaction, in which amino groups react with ninhydrin, leading to formation of purple diketohydrindylidene diketohydrindamine (DYDA) [36]. Results in Fig. S4 showed that the intensity of DYDA color was reduced after conjugation of AMD3100, which consumed amino groups in BAM. Conjugation of AMD3100 did not alter the morphology of BAM NPs (Fig. 3c). Consistently, the resulting AMD3100-conjugated BAM NPs, designated as A-BAM NPs, responded to acidic pH by releasing payloads in an accelerated rate (Fig. S6, Supporting Information). A-BAM NPs were tested in mice for drug delivery to the ischemic brain. NPs were synthesized with encapsulation of IR780, a near-infrared dye allowing for non-invasive imaging, and administered intravenously to mice after MCAO surgery.
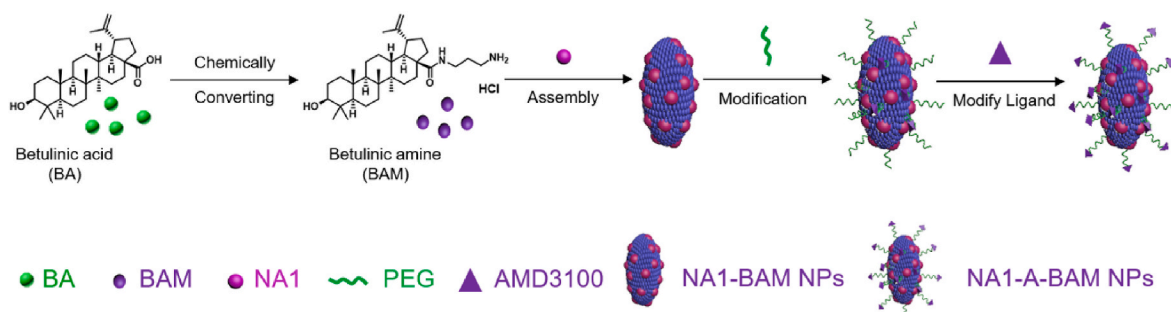
Scheme 1. Schematic diagram of NA1-A-BAM NP synthesis.
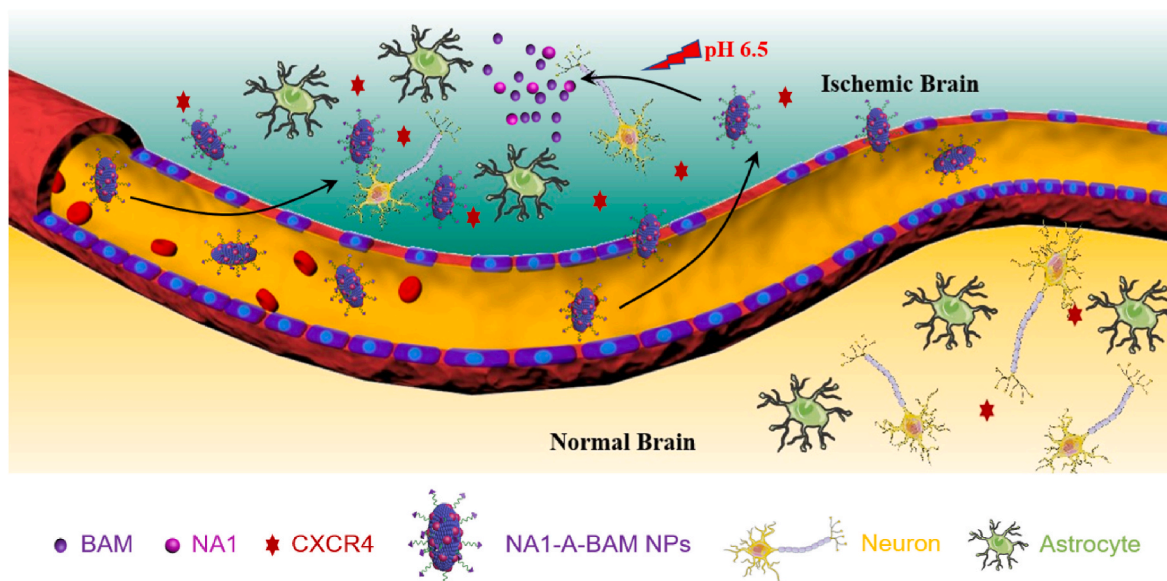
Scheme 2. Schematic diagram of application of NA1-A-BAM NPs for stroke treatment.
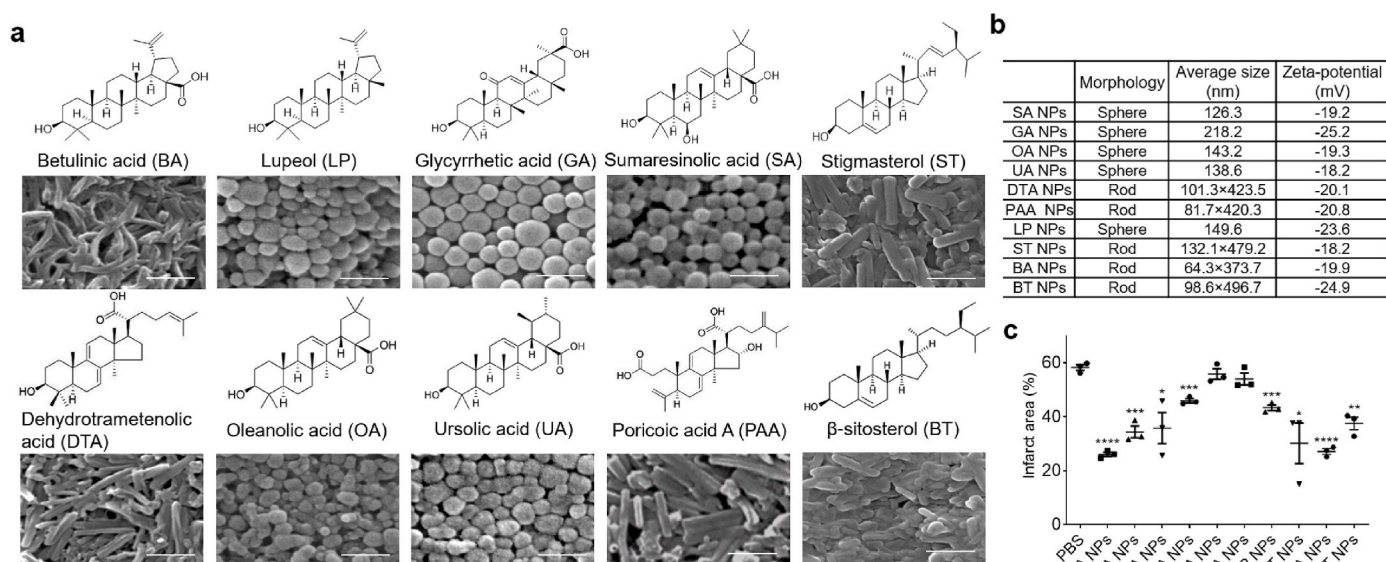

Fig. 1. Screen of natural nanomaterials for stroke treatment. a) Molecular structures of the selected natural nanomaterials and their derived NPs. Scale bar: 500 nm. b) Characteristics of NPs derived from the indicated nanomaterials. c) Quantification of the percentage of infarct area in the brain of stroke mice receiving treatment of the indicated NPs 3 days after MCAO surgery. Data are presented as mean $\pm$ SD (n = 3; *$P < 0.05$, **$P < 0.01$, ***$P < 0.001$, ****$P < 0.0001$. t-test).

Control mice received treatment of IR780-loaded BA NPs, BAM NPs without modification, or BAM NPs with PEG but not AMD3100. The amount of NPs was normalized to ensure that each mouse received the same amount of IR780. Twenty-four hours after treatment, the mice were imaged and then euthanized. The brains were harvested and imaged. We found that, among all the tested NPs, A-BAM NPs demonstrated the greatest efficiency. Based on the fluorescence intensity, the amount of A-BAM NPs accumulated in the ischemic region was 3.2-, 2.5-, and 1.7-fold greater than that of BA NPs, BAM NPs, and BAM NPs with PEG, respectively (Fig. 3d and e). *Ex vivo* imaging of major organs demonstrated that the amount of A-BAM NPs accumulated in ischemic region of the brain was significantly greater than that in the liver, where NPs typically accumulate the most (Fig. S7a, Supporting Information). Compared to that in other organs, the clearance of NPs in the ischemic brain tissue was at a faster rate. By the end of day 3, most A-BAM NPs in the brain were cleared, while the amount of NPs in other organs

remained high (Fig. S7a, Supporting Information). The fast clearance in the ischemic brain is likely due to the accelerated degradation of A-BAM NPs in acidic ischemic tissue. In addition to the high efficiency, A-BAM NPs showed a high degree specificity to the ischemic region, evidenced by the overlap of the location of ischemia (white, TTC staining) with the location of NPs (red to yellow, IR780 signal) (Fig. 3f). The high degree of specificity could be attributed to the interaction of NPs with CXCR4, as confocal microscopic analysis revealed co-localization of NPs with CXCR4 in ischemic tissue (Fig. S7b, Supporting Information).

3.5. Evaluation of A-BAM NPs as a therapeutic for stroke treatment

We evaluated A-BAM NPs for treatment of stroke. Mice received MCAO surgery were administered with A-BAM NPs at 1 mg intravenously. Control mice were treated with PBS. Treatments were performed for three times at 0, 24, and 48 h after surgery. The mice were monitored
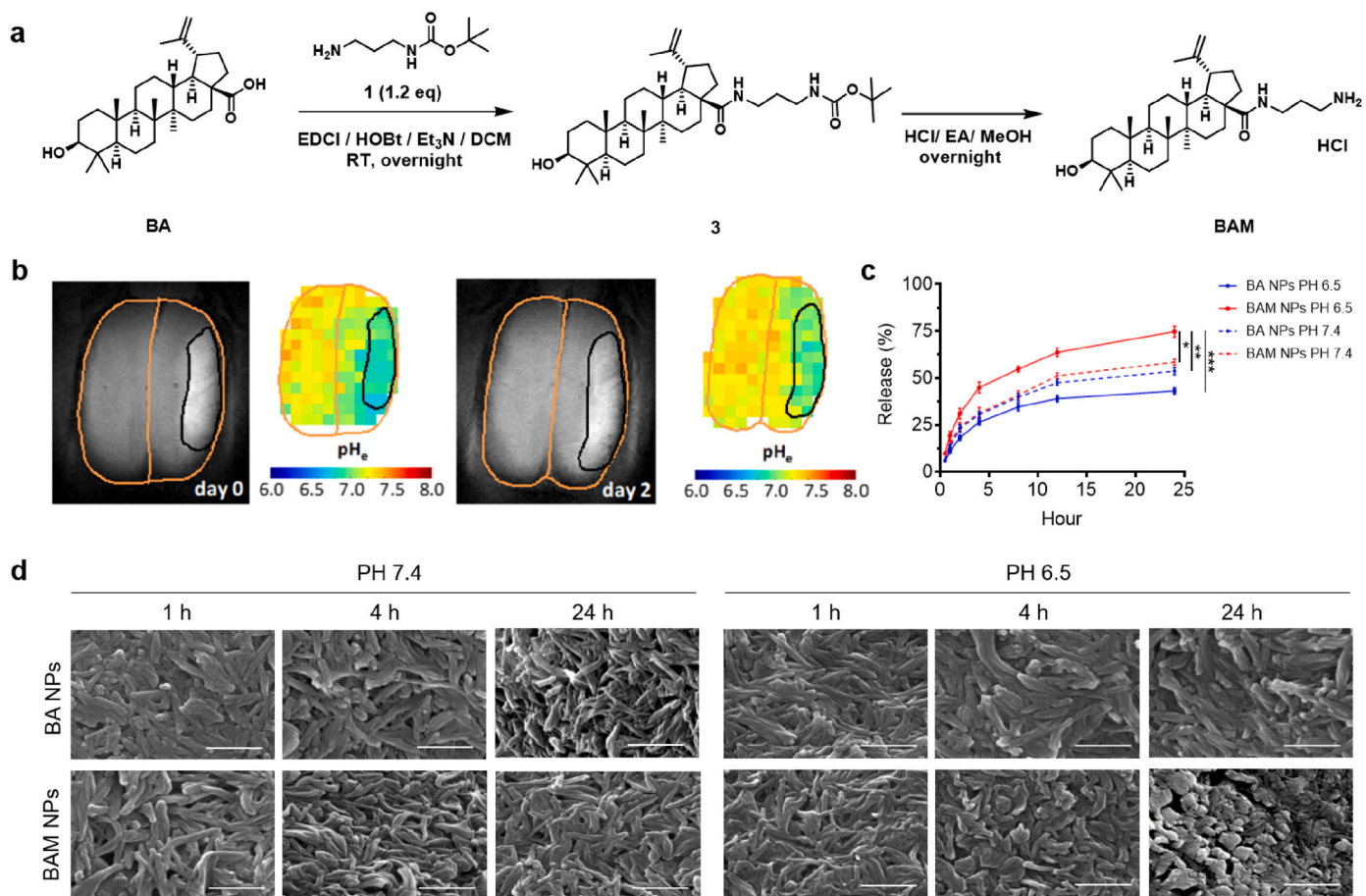
Fig. 2. Development of BAM NPs for acid-triggered drug release. a) Scheme of BAM synthesis. b) Distribution of pH in the brain at day 0 and day 2 after ischemic insult as determined by BIRDS. c) Release of IR780, a model payload, from BA or BAM NPs with time at pH 6.5 or pH 7.4. d) SEM analysis of morphological changes of BA or BAM NPs after incubation at pH 6.5 or pH 7.4 for the indicated time. Scale bar: 500 nm. Data are presented as mean ± SD (n = 3; *$P < 0.05$, **$P < 0.01$, ***$P < 0.001$. t-test).
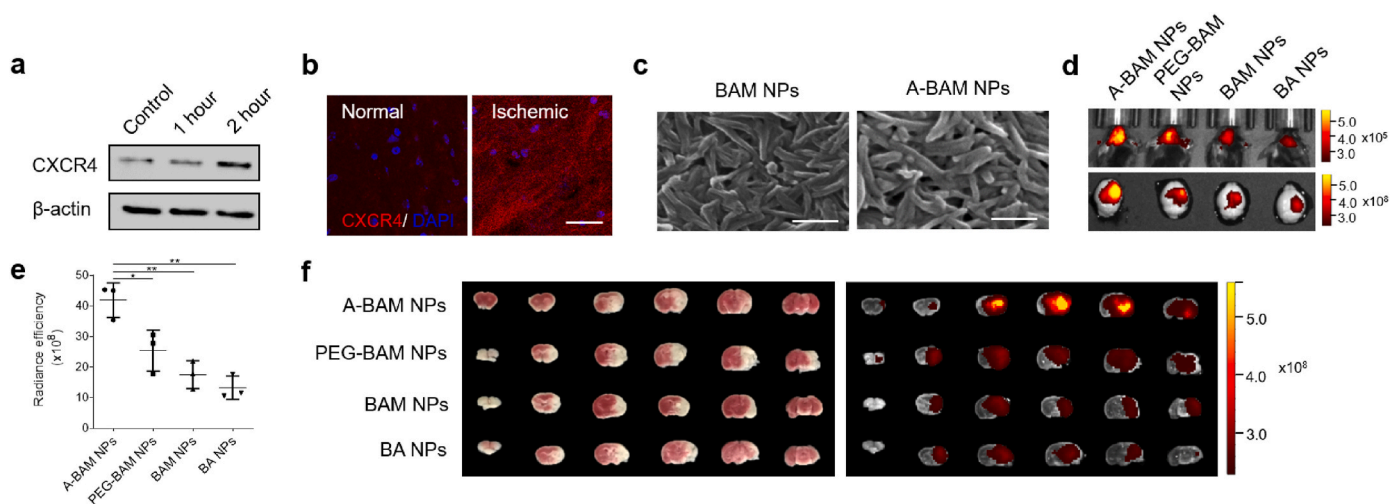

Fig. 3. Synthesis and characterization of A-BAM NPs for targeted drug delivery to stroke. a) Western blot analysis of the expression of CXCR4 in ischemic brain tissue at the indicated time. Control: normal brain tissue. b) Representative images of CXCR4 expression in the region normal or ischemic brain tissue. Scale bar: 30 μm. c) Morphology of BAM NPs with and without AMD3100-conjugation as determined by SEM. d-e) Representative images (d) and semi-quantification (e) of the indicated NPs in the brain of stroke mice after intravenous administration. f) Representative images of brain slices with TTC staining of ischemia (left) and fluorescence imaging of IR780 (right). Data are presented as mean ± SD (n = 3; *$P < 0.05$, **$P < 0.01$. t-test).

for survival daily and assessed for neurological scores on day 3. A separate cohort of mice receiving the same treatment was euthanized on day 3 after surgery to determine the change of infarct area. We found that treatment with A-BAM NPs significantly reduced infarct volumes by 57.1% (Fig. 4a and b), enhanced the survival of mice (Fig. 4c, $p < 0.01$), and improved neurological scores (Fig. 4d). Our previous study showed that the amount of AMD3100 used as a ligand was insufficient to produce biological effects [17]. Therefore, the observed therapeutic effects of A-BAM NPs can be attributed to the antioxidant effect BAM (Fig. S8, Supporting Information), which was found to be comparable to the natural form of BA [10].

We assessed if intravenous administration of A-BAM NPs or NA1-A-BAM NPs induced systemic toxicity. Mice were treated with NPs at 1 mg through tail vein injection. On day 1 and day 7 after treatment, blood samples were collected and subjected to serum aspartate aminotransferase (AST) and alanine aminotransferase (ALT) analyses. Results in Figs. S9a and b showed that intravenous administration of A-BAM NPs and NA1-A-BAM NPs did not induce significant hepatic toxicity. Further H&E analyses of major organs did not detect obvious tissue damage (Fig. S9c, Supporting Information). These results suggest that A-BAM NPs and NA1-A-BAM NPs might be safe for intravenous administration.

3.6. Evaluation of A-BAM NPs as a carrier for delivery of stroke therapeutics

We characterized A-BAM NPs as a carrier for targeted delivery of NA1 for stroke treatment. NA1 is a fusion peptide, which includes TAT at the N terminal and NR2B9c at the C-terminal, and is designed to disrupt nNOS-PSD-95 interaction. In the recently completed ESCAPE clinical trial [19], NA1 demonstrated therapeutic benefits in some patients. However, its efficacy was diminished in patients who received tPA treatment. The results may not be a surprise as free NA1 is not optimal for stroke treatment. First, TAT peptide is highly positively charged and can non-specifically bind to tPA, leading to loss of NA1 bioactivity. Second, NA1 is not designed to penetrate the brain. Due to non-specific binding, the amount of NA1 that can reach the brain after intravenous injection could be limited. Both limitations can be potentially overcome through delivery via nanocarriers. To test the hypothesis, we synthesized A-BAM NPs with encapsulation of NA1. The resulting NA1-loaded A-BAM NPs, or NA1-A-BAM NPs, contained NA1 at 5% by weight. This degree of encapsulation was chosen to allow for delivery of NA1 at 1 nM/g, a subtherapeutic dose [37], when A-BAM NPs were administered at 1 mg. Analysis by SEM and TEM showed that encapsulation of NA1 did not alter the shape and size of A-BAM NPs (Fig. 5a). A-BAM NPs released over 91% of NA1 within 48 h at pH 6.5; in contrast, only 53% of NA1 was released at physiological pH (Fig. 5b). Following the same procedures that were used for evaluation of A-BAM NPs, we evaluated NA1-A-BAM NPs in stroke-bearing mice. Results in Fig. 5c–e showed that treatment with NA1-A-BAM NPs demonstrated a therapeutic benefit greater than A-BAM NPs without NA1 encapsulation across all the three

characterization criteria. The difference in neurological score did not meet significance, likely because the standard 5-point scale behavior test is not sensitive enough for measuring complicated neurological functions. We found that treatment with NA1-A-BAM NPs significantly increased the survival (Fig. 5c, $p < 0.01$), reduced infarct volumes by 69.8% (Fig. 5d and Fig. S11, Supporting Information), and enhanced neurological scores (Fig. 5e). Mechanistically, treatment with NA1-A-BAM NPs disrupted nNOS-PSD-95 coupling in efficiency significantly greater than treatment with A-BAM NPs without NA1 encapsulation; in addition, the treatment significantly decreased BBB leakage, improved tight junction repair, and reduced brain edema (Fig. S10, Supporting Information). Lastly, we showed that infusion of tPA did not reduce the efficacy of NA1 when delivered using A-BAM NPs (Fig. S11, Supporting Information). Collectively, these results indicated that delivery via A-BAM NPs enhances the efficacy of NA1, and treatment with NA1-A-BAM NPs is compatible with tPA infusion.

4. Discussion

Improved treatment of stroke requires development of novel therapeutics which need not only to cross the BBB to the ischemic brain, but also to modulate multiple complementary targets [5–7]. To achieve this goal, we screened a collection of natural nanomaterials and identified BA as one of the most potent antioxidants for stroke treatment (Fig. 1). We engineered BA NPs to enable acid-triggered drug release and targeted delivery to the ischemic brain and demonstrated that the resulting A-BAM NPs can not only be used as a therapeutic agent for stroke treatment but also employed as a carrier for drug delivery to the ischemic brain. As a therapeutic agent, A-BAM NPs effectively reduce cerebral infarction after intravenous administration (Fig. 4). Since ischemia alters the metabolic phenotype to anaerobic glycolysis, we found that the stroked region is within acidic pH range suitable for the rapid acid-triggered drug release of BAM NPs (Fig. 2). The efficacy of A-BAM NP treatment is superior than that of BA NPs in their natural form [10]. This is likely due to two reasons. First, BAM has a greater antioxidant effect than BA (Fig. S8, Supporting Information). Second, compared to BA NPs, A-BAM NPs penetrate the brain with higher efficiency (Fig. 3d and e). As a delivery vehicle, A-BAM NPs can efficiently carry payloads to the brain and release therapeutics preferentially in the ischemic microenvironment at a fast rate (Fig. 2a,c). This dual functionality makes A-BAM NPs distinct from those NPs documented in the literature, acting solely as carriers (Table S1, Supporting Information).

We showed that delivery via A-BAM NPs can both enhance the efficacy of NA1 and enable NA1 therapy to be compatible with tPA infusion (Fig. S11, Supporting Information). NA1 contains NR2B9c, the functional unit, and TAT, which is employed to deliver NA1 to the brain and into targeted cells [18]. One major limitation of using TAT is the lack of specificity, as this highly positively charged peptide can bind to negatively charged proteins and cells throughout the circulatory system [38,39]. This limitation likely causes two major problems. First, due to
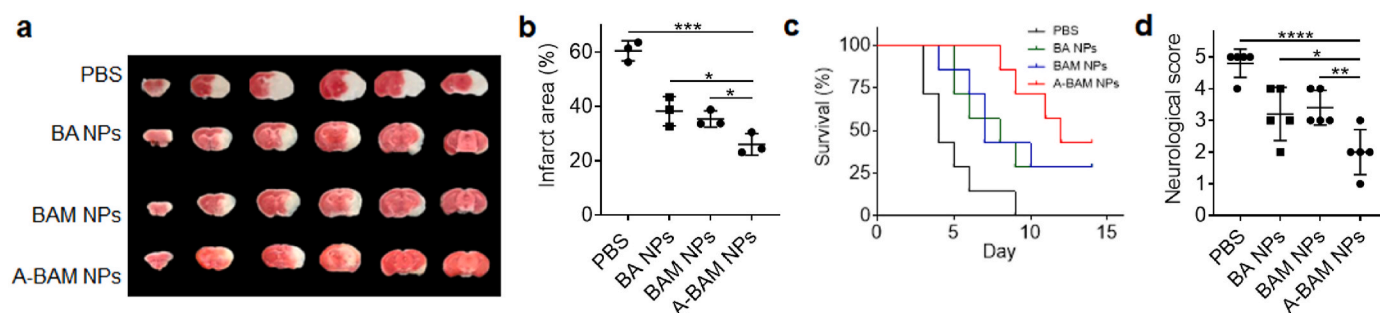

Fig. 4. Evaluation of A-BAM NPs as a therapeutic agent for stroke treatment. a-d) Representative images a) and quantification b) of cerebral infarction (n = 3), c) Kaplan−Meier survival analysis (n = 7), and d) neurological scores (day 3 after surgery, n = 5) of stroke mice receiving the indicated treatments. Infarct area and neurological scores were determined on day 3 after surgery. Data are presented as mean ± SD (*$P < 0.05$, **$P < 0.01$, ***$P < 0.001$, ****$P < 0.0001$. t-test).
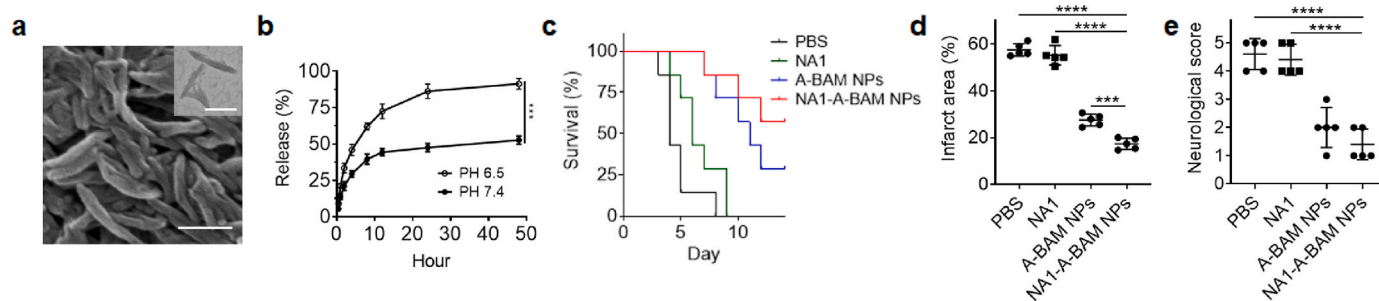
Fig. 5. Characterization of A-BAM NPs for targeted delivery of NA1 for stroke treatment. a) Representative images of NA1-A-BAM NPs by SEM (Scare bar: 200 nm) and TEM (inset, scare bar: 100 nm). b) Release of NA1 from NA1-A-BAM NPs with time at the indicated pH. c) Kaplan–Meier survival analysis (n = 7), d) infarct area (n = 5), and e) neurological scores (day 3 after surgery, n = 5) of stroke mice receiving the indicated treatments. Infarct area and neurological scores were determined on day 3 after surgery. Data are presented as mean ± SD (***$P < 0.001$, ****$P < 0.0001$. t-test).

the non-specific interaction, NA1 needs to be administered at a high dose to achieve significant therapeutic benefits. In previous mouse studies, no therapeutic effects could be achieved unless NA1 was administered at doses greater than 10 nM/g [37]. In this study, we showed that NA1 at a subtherapeutic dose of 1 nM/g, which by itself has no efficacy, provided significant therapeutic benefits when delivered via A-BAM NPs (Fig. 5c–e), and the efficacy is not worse than higher doses in various animal stroke models (Table S2, Supporting Information). Therefore, the bioequivalence of NA1-loaded A-BAM NPs is at least 10 times over free NA1. Second, the non-specific binding may be responsible for the incompatibility observed in the recently completed ESCAPE clinical trial, in which NA1 failed to demonstrate therapeutic benefits when tPA was co-administered [19]. It is likely that the highly positively charged TAT peptide mediates binding between NA1 and tPA. The binding, in turn, prevents NA1 from penetrating the brain, leading to loss of NA1 activities. This hypothesis is supported by our observation that co-administration of tPA did not reduce the efficacy of NA1, when NA1 was encapsulated and delivered via A-BAM NPs (Fig. S11, Supporting Information).

In addition to its antioxidant effects, BA is known have antiviral, antidiabetic, antihyperlipidemic, and anti-inflammatory activities [40]. In addition to the major component, AMD3100 as the ligand is also known to have pharmacological activities by targeting the CXCR4/CXCL12 pathway [41,42]. Therefore, it is likely that A-BAM NPs can be utilized for management of more diseases other than stroke.

5. Conclusion

In conclusion, we designed and synthesized A-BAM NPs to enable targeted delivery to the ischemic brain with high efficiency and accelerated drug release preferentially to ischemic brain tissue. We demonstrated that A-BAM NPs can be employed as an antioxidant agent for stoke treatment as well as a carrier to improve the therapeutic benefits of NA1. Due to their multifunctionality and significant efficacy, we anticipate that A-BAM NPs have great potential to be translated into clinical applications both as a therapeutic and as a drug carrier for stroke treatment.

Data availability

All relevant data supporting the flndings of this study are either included within the article and its Supplementary Information files or available upon request from the corresponding author.

CRediT authorship contribution statement

Shenqi Zhang: Methodology, Investigation, Writing – original draft. **Bin Peng:** Methodology, Investigation, Writing – original draft. **Zeming Chen:** Methodology, Investigation. **Jiang Yu:** Methodology,

Investigation. **Gang Deng:** Methodology, Investigation. **Youmei Bao:** Methodology, Investigation. **Chao Ma:** Methodology, Investigation. **Fengyi Du:** Methodology, Investigation. **Wendy C. Sheu:** Methodology, Investigation. **W. Taylor Kimberly:** Resources. **J. Marc Simard:** Resources. **Daniel Coman:** Methodology, Investigation, Writing – original draft. **Qianxue Chen:** Resources. **Fahmeed Hyder:** Resources, Supervision, Funding acquisition. **Jiangbing Zhou:** Conceptualization, Resources, Writing – review & editing, Supervision, Funding acquisition. **Kevin N. Sheth:** Resources, Writing – review & editing, Supervision, Funding acquisition.

Declaration of competing interest

The authors declare that they have no known competing financial interests or personal relationships that could have appeared to influence the work reported in this paper.

Acknowledgements

Appendix A. Supplementary data

Supplementary data to this article can be found online at https://doi.org/10.1016/j.bioactmat.2022.02.033.

References

[1] S. Virani, A. Alonso, E. Benjamin, M. Bittencourt, C. Callaway, A. Carson, et al., Heart disease and stroke statistics-2020 update: a report from the American heart association, Circulation 141 (2020) e139–e596.

[2] L. Schwamm, S. Ali, M. Reeves, E. Smith, J. Saver, S. Messe, et al., Temporal trends in patient characteristics and treatment with intravenous thrombolysis among acute ischemic stroke patients at Get with the Guidelines-Stroke hospitals, Circulation Cardiovascular quality and outcomes 6 (2013) 543–549.

[3] T. Patel, J. Zhou, J. Piepmeier, W. Saltzman, Polymeric nanoparticles for drug delivery to the central nervous system, Adv. Drug Deliv. Rev. 64 (2012) 701–705.

[4] V. Bharadwaj, D. Nguyen, V. Kodibagkar, S. Stabenfeldt, Nanoparticle-based therapeutics for brain injury, Adv. Healthc. Mater. 7 (2018) 1700668.

[5] L. Han, Q. Cai, D. Tian, D. Kong, X. Gou, Z. Chen, et al., Targeted drug delivery to ischemic stroke via chlorotoxin-anchored, lexiscan-loaded nanoparticles, Nanomed. Nanotechnol. Biol. Med. 12 (2016) 1833–1842.

[6] T. Luo, J. Wang, S. Hao, T. Guo, P. Ren, Z. Cheng, et al., Brain drug delivery systems for the stroke intervention and recovery, Curr. Pharmaceut. Des. 23 (2017) 2258–2267.

[7] J. Meschia, T. Brott, Ischaemic stroke, Eur. J. Neurol. 25 (2018) 35–40.

[8] X. Yang, C. Ma, Z. Chen, J. Liu, F. Liu, R. Xie, et al., Single small molecule-assembled nanoparticles mediate efficient oral drug delivery, Nano Res. 12 (2019) 2468–2476.

[9] Y. Bao, S. Zhang, Z. Chen, A. Chen, J. Ma, G. Deng, et al., Synergistic chemotherapy for breast cancer and breast cancer brain metastases via paclitaxel-loaded oleanolic acid nanoparticles, Mol. Pharm. 17 (2020) 1343–1351.

[10] G. Deng, C. Ma, H. Zhao, S. Zhang, J. Liu, F. Liu, et al., Anti-edema and antioxidant combination therapy for ischemic stroke via glyburide-loaded betulinic acid nanoparticles, Theranostics 9 (2019) 6991–7002.

[11] Y. Xie, C. Ma, X. Yang, J. Wang, G. Long, J. Zhou, Phytonanomaterials as therapeutic agents and drug delivery carriers, Adv. Drug Deliv. Rev. (2021) 113868.

[12] Z. Wang, Y. Han, S. Tian, J. Bao, Y. Wang, J. Jiao, Lupeol alleviates cerebral ischemia-reperfusion injury in correlation with modulation of PI3K/akt pathway, Neuropsychiatric Dis. Treat. 16 (2020) 1381–1390.

[13] H. Chen, B. Guan, B. Wang, H. Pu, X. Bai, X. Chen, et al., Glycyrrhizin prevents hemorrhagic transformation and improves neurological outcome in ischemic stroke with delayed thrombolysis through targeting peroxynitrite-mediated HMGB1 signaling, Transl Stroke Res 11 (2020) 967–982.

[14] J. Sun, X. Li, J. Liu, X. Pan, Q. Zhao, Stigmasterol exerts neuro-protective effect against ischemic/reperfusion injury through reduction of oxidative stress and inactivation of autophagy, Neuropsychiatric Dis. Treat. 15 (2019) 2991–3001.

[15] L. Caltana, M.L. Nieto, A. Brusco, Oleanolic acid: a promising neuroprotective agent for cerebral ischemia, Neural regeneration research 10 (2015) 540–541.

[16] Y. Wang, L. Li, S. Deng, F. Liu, Z. He, Ursolic acid ameliorates inflammation in cerebral ischemia and reperfusion injury possibly via high mobility group box 1/toll-like receptor 4/NFkappaB pathway, Front. Neurol. 9 (2018) 253.

[17] X. Guo, G. Deng, J. Liu, P. Zou, F. Du, F. Liu, et al., Thrombin-responsive, brain-targeting nanoparticles for improved stroke therapy, ACS Nano 12 (2018) 8723–8732.

[18] M. Aarts, Y. Liu, L. Liu, S. Besshoh, M. Arundine, J.W. Gurd, et al., Treatment of ischemic brain damage by perturbing NMDA receptor- PSD-95 protein interactions, Science 298 (2002) 846–850.

[19] M.D. Hill, M. Goyal, B.K. Menon, R.G. Nogueira, R.A. McTaggart, A.M. Demchuk, et al., Efficacy and safety of nerinetide for the treatment of acute ischaemic stroke (ESCAPE-NA1): a multicentre, double-blind, randomised controlled trial, Lancet 395 (2020) 878–887.

[20] G. Deng, C. Ma, H. Zhao, S. Zhang, J. Liu, F. Liu, et al., Anti-edema and antioxidant combination therapy for ischemic stroke via glyburide-loaded betulinic acid nanoparticles, Theranostics 9 (2019) 6991–7002.

[21] L. Han, Q. Cai, D. Tian, D.K. Kong, X. Gou, Z. Chen, et al., Targeted drug delivery to ischemic stroke via chlorotoxin-anchored, lexiscan-loaded nanoparticles, Nanomedicine 12 (2016) 1833–1842.

[22] J. Ma, S. Zhang, J. Liu, F. Liu, F. Du, M. Li, et al., Targeted drug delivery to stroke via chemotactic recruitment of nanoparticles coated with membrane of engineered neural stem cells, Small 15 (2019), e1902011.

[23] Q. Cai, Z. Chen, D.K. Kong, J. Wang, Z. Xu, B. Liu, et al., Novel microcatheter-based intracarotid delivery approach for MCAO/R mice, Neurosci. Lett. 597 (2015) 127–131.

[24] D. Coman, Y. Huang, J.U. Rao, H.M. De Feyter, D.L. Rothman, C. Juchem, et al., Imaging the intratumoral-peritumoral extracellular pH gradient of gliomas, NMR Biomed. 29 (2016) 309–319.

[25] D. Coman, H.K. Trubel, R.E. Rycyna, F. Hyder, Brain temperature and pH measured by (1)H chemical shift imaging of a thulium agent, NMR Biomed. 22 (2009) 229–239.

[26] D. Coman, R.A. de Graaf, D.L. Rothman, F. Hyder, In vivo three-dimensional molecular imaging with Biosensor Imaging of Redundant Deviation in Shifts (BIRDS) at high spatiotemporal resolution, NMR Biomed. 26 (2013) 1589–1595.

[27] M. Nedergaard, R.P. Kraig, J. Tanabe, W.A. Pulsinelli, Dynamics of interstitial and intracellular pH in evolving brain infarct, Am. J. Physiol. 260 (1991) R581–R588.

[28] E.M. Nemoto, S. Frinak, Brain tissue pH after global brain ischemia and barbiturate loading in rats, Stroke 12 (1981) 77–82.

[29] J.Y. Zhou, J.F. Payen, D.A. Wilson, R.J. Traystman, P.C.M. van Zijl, Using the amide proton signals of intracellular proteins and peptides to detect pH effects in MRI, Nat. Med. 9 (2003) 1085–1090.

[30] P.Z. Sun, E. Wang, J.S. Cheung, Imaging acute ischemic tissue acidosis with pH-sensitive endogenous amide proton transfer (APT) MRI–correction of tissue relaxation and concomitant RF irradiation effects toward mapping quantitative cerebral tissue pH, Neuroimage 60 (2012) 1–6.

[31] P.Z. Sun, J.Y. Zhou, W.Y. Sun, J. Huang, P.C.M. van Zijl, Detection of the ischemic penumbra using pH-weighted MRI, J Cerebr Blood F Met 27 (2007) 1129–1136.

[32] Y. Huang, D. Coman, P. Herman, J.U. Rao, S. Maritim, F. Hyder, Towards longitudinal mapping of extracellular pH in gliomas, NMR Biomed. 29 (2016) 1364–1372.

[33] D. Coman, D.C. Peters, J.J. Walsh, L.J. Savic, S. Huber, A.J. Sinusas, et al., Extracellular pH mapping of liver cancer on a clinical 3T MRI scanner, Magn. Reson. Med. 83 (2020) 1553–1564.

[34] S. Zhang, G. Deng, F. Liu, B. Peng, Y. Bao, F. Du, et al., Autocatalytic delivery of brain tumor-targeting, size-shrinkable nanoparticles for treatment of breast cancer brain metastases, Adv. Funct. Mater. 30 (2020) 1910651.

[35] Y. Wang, Y. Xie, D. Oupicky, Potential of CXCR4/CXCL12 chemokine Axis in cancer drug delivery, Curr Pharmacol Rep 2 (2016) 1–10.

[36] P.A. Kendall, Use of the ninhydrin reaction for quantitative estimation of amino groups in insoluble specimens, Nature 197 (1963) 1305–1306.

[37] L. Teves, H. Cui, M. Tymianski, Efficacy of the PSD95 inhibitor Tat-NR2B9c in mice requires dose translation between species, J. Cerebr. Blood Flow Metabol. 36 (2016) 555–561.

[38] X. Yu, X. Gou, P. Wu, L. Han, D. Tian, F. Du, et al., Activatable protein nanoparticles for targeted delivery of therapeutic peptides, Adv. Mater. 30 (2018) 1705383.

[39] H. Derakhshankhah, S. Jafari, Cell penetrating peptides: a concise review with emphasis on biomedical applications, Biomed. Pharmacother. 108 (2018) 1090–1096.

[40] J.L. Rios, S. Manez, New pharmacological opportunities for betulinic acid, Planta Med. 84 (2018) 8–19.

[41] A.J. Shepherd, L. Loo, R.P. Gupte, A.D. Mickle, D.P. Mohapatra, Distinct modifications in Kv2.1 channel via chemokine receptor CXCR4 regulate neuronal survival-death dynamics, J. Neurosci. 32 (2012) 17725–17739.

[42] X. Huang, M. Wan, Q. Yang, X. Ding, Z. Zhou, The stromal cell-derived factor-1 alpha (SDF-1alpha)/cysteine-X-cysteine chemokine receptor 4 (CXCR4) axis: a possible prognostic indicator of acute ischemic stroke, J. Int. Med. Res. 47 (2019) 1897–1907.